Nanoscale Horizons

ROYAL SOCIETY OF CHEMISTRY

COMMUNICATION

View Article Online
View Journal

Cite this: DOI: 10.1039/d6nh00084c

Received 24th February 2026,
Accepted 28th April 2026

DOI: 10.1039/d6nh00084c

rsc.li/nanoscale-horizons

TEM analysis of dicarboxylic acid-induced transition from unilamellar to multilamellar MEL-A vesicles

Tran Ngoc Linh, *[a] Hirohmi Watanabe,[a] Takashi Arimura [b] and Masato Kawasaki[c]

The internal structure of vesicles formed solely by mannosylerythritol lipid-A (MEL-A), a glycolipid produced by basidiomycetous yeasts of the genus *Pseudozyma*, was visualized by liquid cell and cryogenic transmission electron microscopy. Moreover, it was shown for the first time that their morphology can be controlled by dicarboxylic acids acting as molecular signals, combined with the pH of the solution. MEL-A formed nano-sized unilamellar vesicles (200 nm diameter, 5 nm bilayer thickness) at pH 7 and pH 4 without dicarboxylic acids. Upon addition of dicarboxylic acids at pH 7, divalent dicarboxylate anions engage with the hydroxyl groups of the erythritol moiety in MEL-A, driving the growth of unilamellar vesicles with diameters of 250–300 nm. At pH 4, the addition of dicarboxylic acids (oxalic, maleic, fumaric or malonic acids), which exist predominantly as monoanions, induced the expansion to micro-sized vesicles (0.8–2.1 μm in diameter) and the transition into a multilamellar structure consisting of up to 18 layers. For oxalic acid, the vesicular membrane exhibited a thickness of 80 nm and consisted of 16 layers, of which both the outermost and the innermost layer thickness was 5 nm. Vesicle multilayering in MEL-A assemblies is driven by cooperative dissociated/undissociated carboxyl interactions in dicarboxylate monoanions.

New concepts

Precise control over vesicle size and morphology is critical for drug pharmacokinetics, cellular uptake, and tumor targeting, yet remains largely inaccessible. Interestingly, subtle pH fluctuations *in vivo* govern key processes, and dicarboxylic acids—reversibly dissociating without altering their molecular framework—are central to energy metabolism, including the tricarboxylic acid cycle. By leveraging the two-step acid dissociation of dicarboxylic acids, we have achieved stepwise modulation of charge states in response to pH changes, which effectively dictates the resulting supramolecular interactions. By inducing bidentate interactions of dicarboxylic acids modulated by their charge states, we report, for the first time, continuous control of **MEL-A** vesicle structures—an outcome not achievable with monocarboxylic acids. Using the degree of dissociation as a signal may enable the development of nanoassemblies that directly decode life-derived signals.

Introduction

Artificial vesicles are widely used as model systems for membrane permeability, intracellular transport, and intercellular communication, as bilayer vesicles encapsulating aqueous compartments can be formed from both phospholipids and synthetic amphiphilic molecules.[1–4] Vesicle fusion is essential for the transfer of membrane components and encapsulated cargoes to target vesicles[5,6] and is governed by supramolecular interactions such as van der Waals forces, metal–ligand coordination, hydrogen bonding, and host–guest interactions.[7–9] However, membrane reorganization in phospholipid systems mediated by small-molecule bridging interactions has, in most cases, resulted in disruptive aggregation.[10]

Mannosylerythritol lipid (**MEL**) is a microbially derived glycolipid biosurfactant, and its high biodegradability and low toxicity have led to increasing interest in its potential applications in the cosmetic[11,12] and pharmaceutical[13–15] fields. Notably, **MEL-A**, which is efficiently produced by basidiomycetous yeasts of the genus *Pseudozyma*, has been reported to exhibit diverse biological activities, including antimicrobial[16,17] and antitumor[18,19] effects.

Nevertheless, basic insights into the internal architecture and bilayer thickness of **MEL**-based micelle- or vesicle-like assemblies in aqueous solution are still lacking. To this end, precise structural control of these soft nanoparticles is

[a] *Organic Materials Diagnosis Research Group, Research Institute for Sustainable Chemistry, National Institute of Advanced Industrial Science and Technology (AIST), 3-11-32, Kagamiyama, Higashihiroshima, Hiroshima 739-0046, Japan. E-mail: tran.linh@aist.go.jp*

[b] *Open Innovation Laboratory for Food and Medicinal Resource Engineering (FoodMed-OIL), National Institute of Advanced Industrial Science and Technology (AIST), Laboratory of Advanced Research D, University of Tsukuba, Tsukuba, Ibaraki 305-0006, Japan*

[c] *Institute of Materials Structure Science, Inter-University Research Institute Corporation High Energy Accelerator Research Organization (KEK), 1-1 Oho, Tsukuba, Ibaraki 305-0801, Japan*

indispensable for uncovering their functional mechanisms and facilitating the development of innovative applications.

The morphology of vesicles self-assembled by amphiphilic molecules has been extensively reported to be closely related to their bioactivity. However, to the best of our knowledge, no study has ever simultaneously achieved both the visualization of the internal structures of vesicles formed exclusively from **MEL-A** and the external-stimuli-induced control of their morphology.[20,21]

In the course of advancing the structural analysis of **MEL-A** assemblies, we identified that under certain conditions, carboxylate anions may contribute to the association state. Dicarboxylic acids, which are core molecules supporting biological energy metabolism from metabolic end products such as oxalic acid to intermediates in the TCA cycle, exhibit dramatic changes in their charge states depending on the pH.[22–25]

In this study, we exploited this charge modulation and identified aliphatic dicarboxylic acids as trigger molecules that induce fusion of **MEL-A**-derived vesicles, leading, for the first time, to the formation of controlled multilamellar structures rather than disruptive aggregation. Systematic analysis of the self-assembly behavior in aqueous media *via* liquid cell transmission electron microscopy (LC-TEM) and cryogenic TEM (cryo-TEM) reveals the potential for structural control through external stimuli. These findings provide critical insights for enhancing surfactant performance and developing advanced supramolecular applications.

Results and discussion

The hydrophobic domain of **MEL-A** is composed of two fatty acyl chains esterified to the hydroxyl groups at the C-2 and C-3 positions of the mannose residue (Fig. 1). The chain length and degree of unsaturation of these acyl chains have been reported to vary according to the carbon sources supplied in the culture medium, such as oils, and to the substrate specificity of the producing organism.[26–28]

The **MEL-A** used in this study was produced and extracted following established procedures,[29] using *Pseudozyma antarctica* as the source strain and culturing it under conditions in which glucose served as the sole carbon source. The self-assembly behavior of this **MEL-A** in aqueous media has not previously been examined.

The critical aggregation concentration (CAC) of **MEL-A** in aqueous solution was determined by a pyrene fluorescence probe method.[30] The CAC was estimated to be about 6.0×10^{-6} M (Fig. S1, SI), consistent with previously reported CAC values for **MEL-A** produced from other carbon sources.[31]

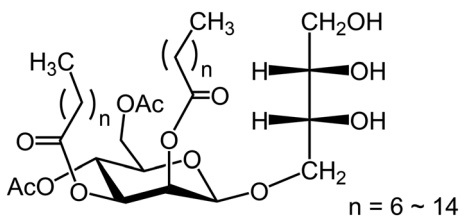

Fig. 1 Chemical structure of **MEL-A**.

Table 1 Hydrodynamic diameter (D)[a], polydispersity index (PDI)[a], and zeta potential (ζ)[b] of **MEL-A** assemblies in buffer solutions at pH 7 and pH 4 (25 °C)

Buffer	[**MEL-A**] (M)	D (nm)	PDI (−)	ζ (mV)
pH 7[c]	4.7×10^{-4}	200 ± 30	0.18 ± 0.02	−16 ± 2
	9.4×10^{-4}	250 ± 20	0.20 ± 0.02	−16 ± 3
	1.9×10^{-3}	300 ± 30	0.25 ± 0.03	−17 ± 3
pH 4[d]	4.7×10^{-4}	200 ± 20	0.16 ± 0.01	−13 ± 3
	9.4×10^{-4}	240 ± 20	0.18 ± 0.02	−14 ± 3
	1.9×10^{-3}	240 ± 30	0.18 ± 0.02	−13 ± 4

[a] Hydrodynamic diameter and PDI were determined by dynamic light scattering (DLS). [b] Zeta potentials were determined by electrophoretic light scattering (ELS). [c] 0.05 M HEPES-KOH buffer (pH 7). [d] 0.05 M glycine/0.005 M acetic acid buffer (pH 4).

The hydrodynamic diameter and zeta potential of **MEL-A** in aqueous solution were measured under conditions of pH 7 and pH 4. All measurements were performed at concentrations above the CAC, specifically at 4.7×10^{-4} M, 9.4×10^{-4} M, and 1.9×10^{-3} M (Table 1).

At a concentration of 4.7×10^{-4} M, the assembly size was 200 nm at both pH 7 and 4, indicating that the effect of solution pH was minimal. When the concentration was increased fourfold to 1.9×10^{-3} M, the size increased to 300 nm at pH 7 and 240 nm at pH 4. This suggests that, at higher concentrations, the collision frequency of assemblies increases, making coalescence more likely. Furthermore, under high-concentration conditions at pH 7, the polydispersity index (PDI) exceeded 0.2, indicating a broader size distribution and a transition to a polydisperse state. Therefore, transmission electron microscopy (TEM) observations of **MEL-A** assemblies were performed at 4.7×10^{-4} M, where the size distribution was relatively uniform.

LC-TEM, enabling *in situ* visualization of dynamic behavior in solution,[32,33] was employed together with cryo-TEM, which provides static structures in the vitrified state, to analyse **MEL-A** assemblies.

The molecular assemblies were found to adopt a vesicle structure with an internal aqueous domain, consistent in size with that determined by dynamic light scattering (DLS) measurements (Fig. 2). The membrane thickness was measured to be about 5 nm, which is about twice the molecular length of **MEL-A** (~2.5 nm). This dimensional relationship strongly suggests that the membrane adopts a bilayer architecture composed of two layers of **MEL-A** molecules.

The zeta potential of **MEL-A** assemblies was −16 ± 2 mV at pH 7 and −13 ± 3 mV at pH 4, showing no significant difference between the two conditions. Furthermore, no effect of the concentration was observed. These results suggest that the composition of the assemblies and the hydration state at the surface remain nearly unchanged regardless of pH conditions.

MEL-A features a sugar-derived polar headgroup and an erythritol-based polar segment (Fig. 1). Even in the absence of

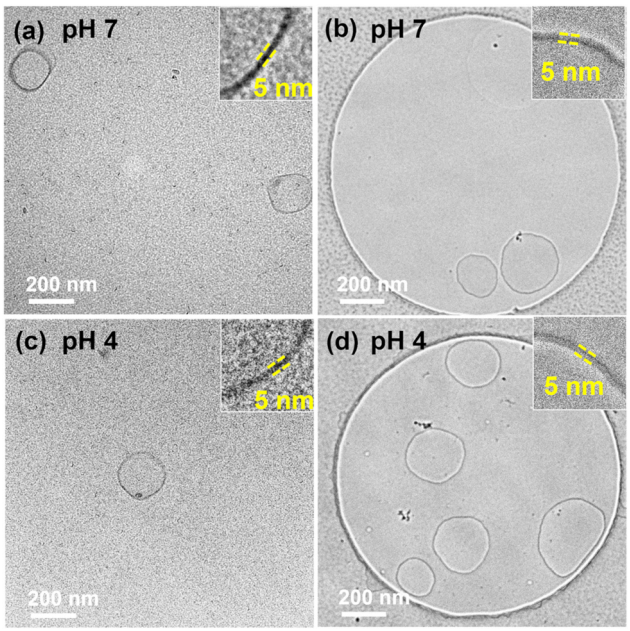

Fig. 2 LC-TEM (a) and (c) and cryo-TEM (b) and (d) images of **MEL-A** assemblies (4.7×10^{-4} M) at pH 7 and pH 4.

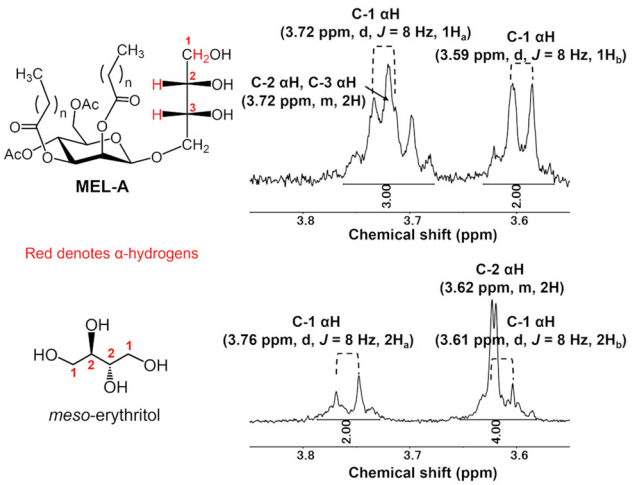

Fig. 3 Partial ^{1}H NMR spectra of **MEL-A** and *meso*-erythritol in D_2O/CD_3OD (40 : 60, v/v) at 25 °C. [**MEL-A**] = [*meso*-erythritol] = 4.7×10^{-4} M.

Table 2 Proton chemical shifts (ppm) of **MEL-A** and *meso*-erythritol in various solvents

	MEL-A[a]			*meso*-Erythritol[a]		
	C-1 αH		C-2 αH	C-1 αH		
Solvent	H_a	H_b	C-3 αH	H_a	H_b	C-2 αH
D_2O	—	—	—	3.77	3.62	3.66
D_2O/CD_3OD (40 : 60)	3.72	3.59	3.72	3.76	3.61	3.62

[a] [**MEL-A**] = [*meso*-erythritol] = 4.7×10^{-4} M.

free hydroxyl groups, the mannose moiety retains the ring oxygen within the pyranose structure and the glycosidic linkage, both contributing to the molecule's polarity.[34] Furthermore, despite the high degree of hydration of the three hydroxyl groups in the erythritol moiety, they can engage in selective interactions with the carboxylate group of a dicarboxylate monoanion when an appropriate hydrophobic local environment is established.[35–38] Therefore, when **MEL-A** forms vesicles, the localization of hydroxyl groups in the vicinity of the hydrophobic interface is expected to promote interactions with the carboxylate groups of dicarboxylate monoanions, thereby leading to a morphological change of the vesicles.

NMR spectroscopy was employed to probe the local polar environment of the hydroxyl groups in the erythritol moiety of **MEL-A**. As hydroxyl protons are not detectable in D_2O, detailed analysis focused on the chemical shifts of the α-protons adjacent to the C-1, C-2, and C-3 positions. In pure D_2O, **MEL-A** self-assembles at 1.0×10^{-4} M, which is above the CAC, resulting in severe peak broadening and precluding meaningful NMR observation. Thus, NMR measurements were performed in the presence of 60% deuterated methanol.

meso-Erythritol was analyzed in D_2O/CD_3OD (40 : 60) as a control. The C-1 α-protons appeared as an AB pattern (J = 8 Hz) at δ 3.76 and 3.61 ppm, with the C-2 α-proton appearing as a multiplet at δ 3.62 ppm. In comparison, **MEL-A** showed the C-1 α-protons at δ 3.72 and 3.59 ppm as a slightly upfield-shifted AB pattern (J = 8 Hz), while the C-2 and C-3 α-protons appeared as a multiplet at δ 3.72 ppm, corresponding to a 0.1 ppm downfield shift relative to *meso*-erythritol (Fig. 3 and Table 2). Previous studies have shown that α-hydrogens next to hydroxyl groups shift downfield near hydrophobic membrane interfaces, influenced by interfacial electric fields and molecular orientation.[39]

Building on this, we hypothesized that the C-2 and C-3 hydroxyl groups of **MEL-A**, when placed in a hydrophobic environment with limited hydration, could interact specifically with the carboxylate group.

Aliphatic dicarboxylic acids from oxalic acid to adipic acid reversibly adopt neutral, monoanionic, or dianionic states depending on pH, while maintaining their carbon skeletons (Table 3 and Table S1). At pH 7, predominantly dianionic dicarboxylic acids were added to **MEL-A** at six equivalents. For strongly acidic species such as oxalic and maleic acids, the vesicle diameter increased from 200 nm to 300 nm, whereas weakly acidic dicarboxylic acids, including glutaric and adipic acids, afforded vesicles of 250 nm in diameter. LC-TEM analysis confirmed that the vesicles retained a unilamellar structure (Fig. S4). The observed enlargement is likely due to association of the dianions with the C-2 and/or C-3 hydroxyl groups at the hydrophobic interface, leading to changes in surface energy and membrane curvature.[40] Moreover, the decrease in the absolute value of the zeta potential upon anion addition can be attributed to a thickened hydration layer, leading to an outward shift of the slipping plane.[41]

To increase the fraction of monovalent anions derived from dicarboxylic acids, in which only one carboxyl group is dissociated, oxalic, maleic, fumaric, or malonic acids were added individually at pH 4. DLS analysis revealed hydrodynamic diameters of 2100 nm, 1500 nm, 1000 nm, and 780 nm,

Table 3 Hydrodynamic diameter (D)[a], polydispersity index (PDI)[a], and zeta potential (ζ)[b] of **MEL-A** assemblies formed in the presence of carboxylic acids[c] at pH 7 and pH 4

			pH 7			pH 4		
Carboxylic acids	pK_{a1}	pK_{a2}	D (nm)	PDI (−)	ζ (mV)	D (nm)	PDI (−)	ζ (mV)
Oxalic acid	1.27	4.27	290 ± 20	0.15 ± 0.03	−12 ± 3	2100 ± 100	0.32 ± 0.10	−5 ± 3
Maleic acid	1.91	6.33	270 ± 30	0.19 ± 0.05	−12 ± 3	1500 ± 100	0.21 ± 0.05	−7 ± 2
Fumaric acid	3.09	4.60	300 ± 20	0.15 ± 0.03	−13 ± 4	1000 ± 70	0.26 ± 0.04	−7 ± 2
Malonic acid	2.83	5.70	250 ± 10	0.12 ± 0.02	−13 ± 3	780 ± 50	0.20 ± 0.02	−8 ± 2
Succinic acid	4.21	5.64	240 ± 10	0.14 ± 0.02	−14 ± 3	300 ± 30	0.05 ± 0.05	−10 ± 3
Glutaric acid	4.34	5.42	250 ± 20	0.15 ± 0.03	−14 ± 4	290 ± 30	0.09 ± 0.04	−10 ± 3
Adipic acid	4.42	5.41	250 ± 10	0.14 ± 0.02	−15 ± 4	250 ± 10	0.09 ± 0.03	−11 ± 3
Propionic acid	4.87	—	220 ± 10	0.10 ± 0.02	−15 ± 3	230 ± 10	0.08 ± 0.01	−12 ± 4

[a] Hydrodynamic diameter and PDI were determined by dynamic light scattering (DLS). [b] Zeta potentials were determined by electrophoretic light scattering (ELS). [c] Measurements were carried out in [**MEL-A**] = 4.7×10^{-4} M and [carboxylic acid] = 3.0×10^{-3} M.

respectively, indicating a pronounced enlargement of giant vesicles in all cases. Given that the fraction of species with both carboxyl groups in the undissociated state is less than 10% at pH 4, this vesicular growth is attributed primarily to the effect of monovalent anions of the dicarboxylic acids. The addition of succinic, glutaric, or adipic acids at pH 4 (where >60% exists in the non-dissociated form) resulted in an increase in vesicular diameter from 200 nm to 250–300 nm, consistent with the results obtained at pH 7. In contrast, the monocarboxylate propionate anion had little effect on the vesicle size (Fig. S5).

The internal structures of the giant vesicles were investigated by cryo-TEM. At pH 4, the addition of dicarboxylic acids, which predominantly exist as monovalent anions, induced a distinct structural evolution of the vesicles. Unilamellar bilayer assemblies stacked in a concentric manner to yield multilamellar structures comprising up to 18 layers (Fig. 4). In the presence of oxalic acid, the total membrane thickness was about 80 nm, with 16 discernible layers: the outermost and innermost membranes were about 5 nm thick, while the 14 sandwiched inner layers were thinner (about 2.5 nm; Fig. 4a). Similar multilamellar vesicles were observed upon addition of maleic, fumaric, or malonic acids, exhibiting total membrane thicknesses of 80–90 nm, corresponding to the stacking of 16 to 18 membrane layers (Fig. 4b–d). The multilamellar growth may arise from bridging interactions of monovalent dicarboxylate anions between **MEL-A** molecules.

In other words, the carboxylate group of the dicarboxylate monoanion interacts with the hydroxyl groups at the C-2 or C-3 positions of the erythritol moiety, whose chemical environment is significantly influenced by the nonpolar character of the vesicular interface (Fig. 5). Concurrently, within the hydrophobic reaction field created by **MEL-A**, the two undissociated carboxylic acid groups are expected to form a hydrogen-bonded dimer, generating a cross-linking motif.[42–44] The existence of such hydrophobic domains at the **MEL-A**-organized

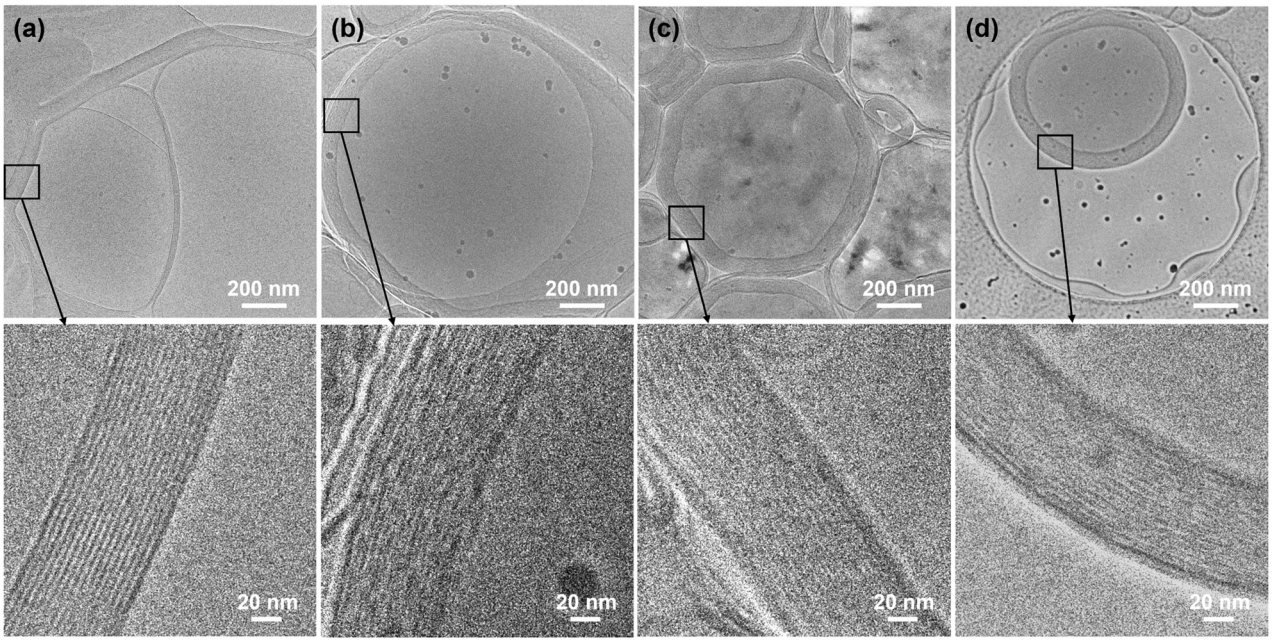

Fig. 4 Cryo-TEM images of **MEL-A** vesicles in the presence of (a) oxalic acid, (b) maleic acid, (c) fumaric acid, and (d) malonic acid at pH 4.

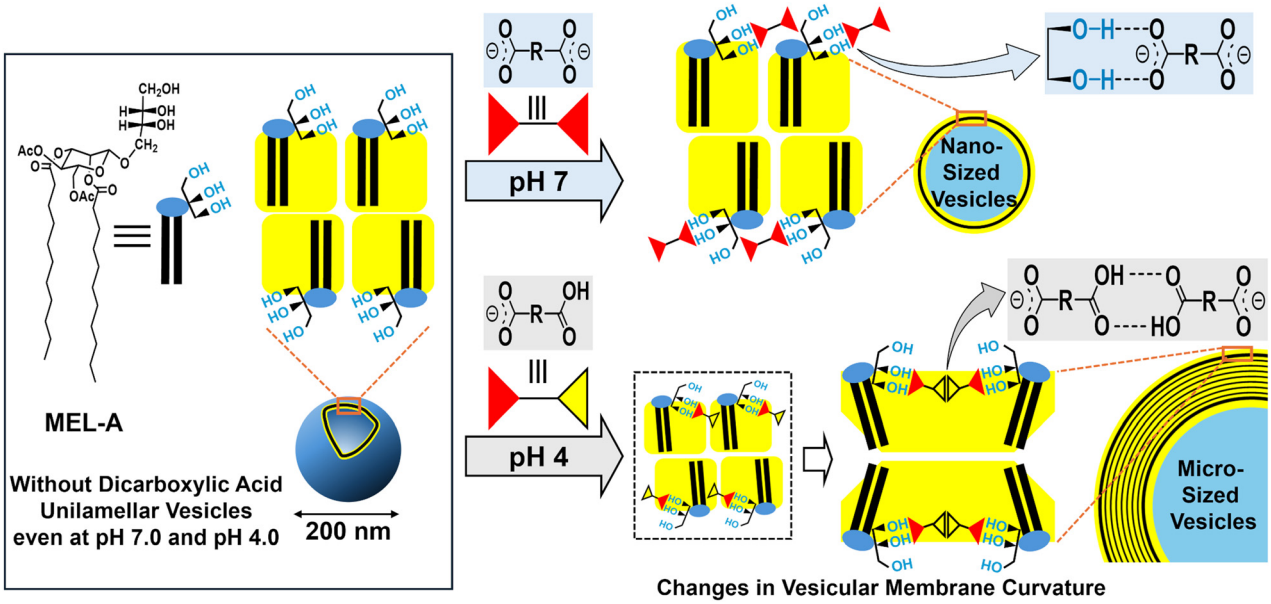

Fig. 5 pH-Dependent dual-site binding of dicarboxylic acids controls **MEL-A** assemblies: nano-sized vesicles at pH 7 and micro-sized vesicles at pH 4. Schematic illustration of a thermodynamic consequence arising from local membrane-curvature changes induced by interactions of pH-responsive dicarboxylic acids.

interface is consistent with fluorescence-probe measurements using pyrene, which indicate an environment more hydrophobic than chloroform (Table S2). These combined interactions of the dicarboxylate monoanion likely bridge multiple **MEL-A** molecules through carboxylic acid hydrogen bonding, leading to substantial changes in membrane curvature and ultimately promoting multilamellar structure formation. However, Fig. 5 provides a conceptual representation illustrating that local variations in membrane curvature can thermodynamically favour the emergence of multilamellar vesicles. While this framework provides a rational basis for the observed structural preference, it does not describe the physical pathways by which individual vesicles reorganize into ordered, concentric multilamellar architectures.

At pH 4, in the presence of succinic acid (38% monoanion/61% non-dissociated) (Table S1), the vesicle diameter expanded to 300 nm. Cryo-TEM imaging revealed structural heterogeneity, where unilamellar vesicles coexist with multilamellar vesicles exhibiting nonuniform membrane thicknesses of 5–80 nm (Fig. 6a). This is likely due to succinic acid monoanions bridging **MEL-A** molecules. Glutaric acid containing 31% of the monocarboxylate anion and adipic acid containing 27% of the monocarboxylate anion do not form multilayered structures (Fig. 6b and c). This behaviour may be attributed to geometric and conformational effects associated with the molecular length and flexibility, which can enhance thermal fluctuations.

In this study, we experimentally demonstrated that dicarboxylic acids interact specifically with vesicle membranes in a pH-responsive manner and, through the resulting modulation of the membrane curvature, ultimately induce the formation of ordered multilamellar vesicle structures. However, the present work primarily focuses on the initial state and the final

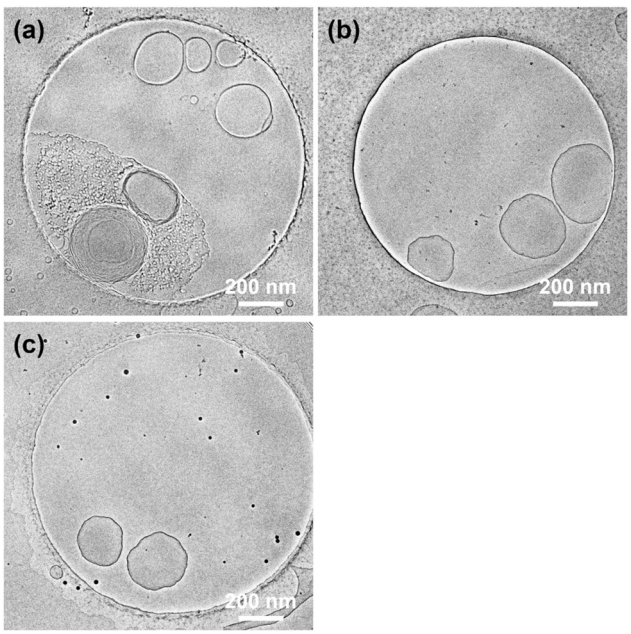

Fig. 6 Cryo-TEM images of **MEL-A** vesicles in the presence of (a) succinic acid, (b) glutaric acid, and (c) adipic acid at pH 4.

structural outcome and does not directly elucidate the time-dependent membrane reorganization dynamics that connect these states. In particular, it remains an open and important question whether the transformation from unilamellar vesicles to multilamellar architectures can be described solely by thermodynamic driving forces or whether it proceeds *via* activated pathways involving rare thermal fluctuations that overcome

local energy barriers. In this context, the thermodynamic–kinetic coupling framework proposed by K. Wang *et al*. offers a promising perspective for extending the mechanistic understanding of the present system.[45] Future studies employing time-resolved measurements, using either label-free or fluorescence-labelled approaches, will be essential to track the temporal evolution of inter-vesicular interactions and membrane reorganization and to discriminate between fusion-driven, adhesion-mediated, or activation-controlled kinetic pathways. In addition, theoretical calculations will be valuable for evaluating interaction length scales and energy barriers at the molecular level. The present study provides an experimental foundation for such future investigations.

Conclusions

Our results indicate that interactions between dicarboxylic acid-derived carboxylate groups and the erythritol moiety of **MEL-A** promote the morphology transition of vesicles. Cooperative interactions between dissociated carboxylate and undissociated carboxylic acid sites in dicarboxylate monoanions are identified, for the first time, as a key factor driving the multilayered organization of **MEL-A**-assembled vesicles. Ongoing work seeks to clarify the relationship between vesicular multilayering and the **MEL-A**-induced membrane curvature.

Tran Ngoc Linh: conceptualization, methodology, investigation, writing – original draft, writing – review & editing, funding acquisition, and visualization. Hirohmi Watanabe: investigation and writing – review & editing. Takashi Arimura: conceptualization, methodology, writing – original draft, and writing – review & editing. Masato Kawasaki: investigation and writing – review & editing.

Conflicts of interest

There are no conflicts to declare.

Data availability

The authors confirm that the data supporting the findings of this study are available within the article and its supplementary information (SI). Supplementary information includes the experimental details, NMR data, additional LC-TEM and cryo-TEM images, vesicle size distributions and histograms of lamellar layer number. See DOI: https://doi.org/10.1039/d6nh00084c.

Acknowledgements

This research was supported by JST grant number JPMJPF2017. We thank Dr T. Morita and Dr A. Saika for helpful discussions and Dr T. Fukuoka for the synthesis and provision of **MEL-A**.

References

1 H. R. Marsden, I. Tomatsu and A. Kros, Model systems for membrane fusion, *Chem. Soc. Rev.*, 2011, **40**, 1572–1585.
2 F. F. Trillo, L. M. Grover, A. S. Brown, P. Harrison and P. M. Mendes, Vesicles in nature and the laboratory: Elucidation of their biological properties and synthesis of increasingly complex synthetic vesicles, *Angew. Chem., Int. Ed.*, 2017, **56**, 3142–3160.
3 H. Pick, A. C. Alves and H. Vogel, Single-vesicle assays using liposomes and cell-derived vesicles: from modeling complex membrane processes to synthetic biology and biomedical applications, *Chem. Rev.*, 2018, **118**, 8598–8654.
4 M. Imai, Y. Sakuma, M. Kurisu and P. Walde, From vesicles toward protocells and minimal cells, *Soft Matter*, 2022, **18**, 4823–4849.
5 J. C. Shillcock and R. Lipowsky, Tension-induced fusion of bilayer membranes and vesicles, *Nat. Mater.*, 2005, **4**, 225–228.
6 A. Grafmuller, J. Shillcock and R. Lipowsky, The fusion of membranes and vesicles: pathway and energy barriers from dissipative particle dynamics, *Biophys. J.*, 2009, **96**, 2658–2675.
7 A. Barba-Bon, M. Nilam and A. Hennig, Supramolecular chemistry in the biomembrane, *ChemBioChem*, 2020, **21**, 886–910.
8 M. Ma and D. Bong, Controlled fusion of synthetic lipid membrane vesicles, *Acc. Chem. Res.*, 2013, **46**, 2988–2997.
9 J. Voskuhl and B. J. Ravoo, Molecular recognition of bilayer vesicles, *Chem. Soc. Rev.*, 2009, **38**, 495–505.
10 M. E. Villanueva, J. Troncoso, P. Losada-Pérez and A. Jover, Impact of amylenes in dipeptide-mediated phospholipid vesicle integrity and aggregation, *J. Mol. Liq.*, 2025, **437**, 128596.
11 T. Morita, T. Fukuoka, T. Imura and D. Kitamoto, Production of mannosylerythritol lipids and their application in cosmetics, *Appl. Microbiol. Biotechnol.*, 2013, **97**, 4691–4700.
12 C. Jing, J. Guo, Z. Li, X. Xu, J. Wang, L. Zhai, J. Liu, G. Sun, F. Wang, Y. Xu, Z. Li, D. Zhao, R. Jiang and L. Sun, Screening and research on skin barrier damage protective efficacy of different mannosylerythritol lipids, *Molecules*, 2022, **27**, 4648.
13 L. Fan, Q. Chen, Y. Mairiyangu, Y. Wang and X. Liu, Stable vesicle self-assembled from phospholipid and mannosylerythritol lipid and its application in encapsulating anthocyanins, *Food Chem.*, 2021, **344**, 128649.
14 D. Liu, G. Liu and S. Liu, Promising application, efficient production, and genetic basis of mannosylerythritol lipids, *Biomolecules*, 2024, **14**, 557.
15 G. Yu, X. Wang, C. Zhang, Z. Chi, Z. Chi and G. Liu, Efficient production of mannosylerythritol lipids by a marine yeast *Moesziomyces aphidis* XM01 and their application as self-assembly nanomicelles, *Mar. Life Sci. Technol.*, 2022, **4**, 373–383.
16 J. Chen, Q. Chen, Q. Shu and Y. Liu, The dual role of mannosylerythritol lipid-A: Improving gelling property and

exerting antibacterial activity in chicken and beef gel, *Food Chem.*, 2025, **464**, 141835.
17 X. Liu, Q. Shu, Q. Chen, X. Pang, Y. Wu, W. Zhou, Y. Wu, J. Niu and X. Zhang, Antibacterial efficacy and mechanism of mannosylerythritol lipids-A on *Listeria monocytogenes*, *Molecules*, 2020, **25**, 4857.
18 J. Meng, C. Yasui, M. Shida, K. Toshima and D. Takahashi, Designed mannosylerythritol lipid analogues exhibiting both selective cytotoxicity against human skin cancer cells and recovery effects on damaged skin cells, *Chem. – Eur. J.*, 2024, **30**, e202401319.
19 Y. Morita, S. Tadokoro, M. Sasai, D. Kitamoto and N. Hirashima, Biosurfactant mannosyl-erythritol lipid inhibits secretion of inflammatory mediators from RBL-2H3 cells, *Biochem. Biophys. Acta*, 2011, **1810**, 1302–1308.
20 L. Fioretto, M. Ziaco, M. Mercogliano, C. Gallo, G. Nuzzo, G. d'Ippolito, D. Castiglia, A. Fontana and E. Manzo, The Janus effect of colloidal self-assembly on the biological response of amphiphilic drugs, *Pharmacol. Res.*, 2024, **208**, 107400.
21 J. A. Doolan, G. T. Williams, K. L. F. Hilton, R. Chaudhari, J. S. Fossey, B. T. Goult and J. R. Hiscock, Advancements in antimicrobial nanoscale materials and self-assembling systems, *Chem. Soc. Rev.*, 2022, **51**, 8696–8755.
22 T. Ermer, L. Nazzal, M. C. Tio, S. Waikar, P. S. Aronson and F. Knauf, Oxalate homeostasis, *Nat. Rev. Nephrol.*, 2023, **19**, 123–138.
23 T. J.-Lahary, T. Shimamura, M. Hayashi, N. Nomura, K. Hirasawa, T. Shimizu, M. Yamashita, N. Tsutsumi, Y. Suehiro, K. Kojima, Y. Sudo, T. Tamura, H. Iwanari, T. Hamakubo, S. Iwata, K. Okazaki, T. Hirai and A. Yamashita, Structure and mechanism of oxalate transporter OxlT in an oxalate-degrading bacterium in the gut microbiota, *Nat. Commun.*, 2023, **14**, 1730.
24 A. C. Roginski, A. B. Zemniaçak, R. A. Marschner, S. M. Wajner, R. T. Ribeiro, M. Wajner and A. U. Amaral, Disruption of mitochondrial functions involving mitochondrial permeability transition pore opening caused by maleic acid in rat kidney, *J. Bioenerg. Biomembr.*, 2022, **54**, 203–213.
25 I. M.-Reyes and N. S. Chandel, Mitochondrial TCA cycle metabolites control physiology and disease, *Nat. Commun.*, 2020, **11**, 102.
26 J. D. D. Almeida, M. F. Nascimento, P. Keković, F. C. Ferreira and N. T. Faria, Unlocking the potential of mannosylerythritol lipids: properties and industrial applications, *Fermentation*, 2024, **10**, 246.
27 D. Liu, G. Liu and S. Liu, Promising application, efficient production, and genetic basis of mannosylerythritol lipids, *Biomolecules*, 2024, **14**, 557.
28 A. Saika, H. Koike, T. Fukuoka and T. Morita, Tailor-made mannosylerythritol lipids: current state and perspectives, *Appl. Microbiol. Biotechnol.*, 2018, **102**, 6877–6884.
29 T. Morita, M. Konishi, T. Fukuoka, T. Imura and D. Kitamoto, Physiological differences in the formation of the glycolipid biosurfactants, mannosylerythritol lipids, between *Pseudozyma antarctica* and *Pseudozyma aphidis*, *Appl. Microbiol. Biotechnol.*, 2007, **74**, 307–315.
30 K. Kalyanasundaram and J. K. Thomas, Environmental effects on vibronic band intensities in pyrene monomer fluorescence and their application in studies of micellar systems, *J. Am. Chem. Soc.*, 1977, **99**, 2039–2044.
31 T. Morita, D. Kawamura, N. Morita, T. Fukuoka, T. Imura, H. Sakai, M. Abe and D. Kitamoto, Characterization of mannosylerythritol lipids containing hexadecatetraenoic acid produced from cuttlefish oil by *Pseudozyma Chrashimaensis* OK96'', *J. Oleo Sci.*, 2013, **62**, 319–327.
32 N. D. Jonge, L. Houben, R. E. D.-Borkowski and F. M. Ross, Resolution and aberration correction in liquid cell transmission electron microscopy, *Nat. Rev. Mater.*, 2019, **4**, 61–78.
33 F. M. Ross, Opportunities and challenges in liquid cell electron microscopy, *Science*, 2015, **350**, aaa9886.
34 J. I. Arutchelvi, S. Bhaduri, P. V. Uppara and M. Doble, Mannosylerythritol lipids: a review, *J. Ind. Microbiol. Biotechnol.*, 2008, **35**, 1559–1570.
35 J. M. Coteron, F. Hacket and H.-J. Schneider, Interactions of Hydroxy Compounds and Sugars with Anions, *J. Org. Chem.*, 1996, **61**, 1429–1435.
36 H.-J. Schneider, L. Tianjun and N. Lomadze, Sensitivity increase in molecular recognition by decrease of the sensing particle size and by increase of the receptor binding site – a case with chemomechanical polymers, *Chem. Commun.*, 2004, 2436–2437.
37 S. Kondo, Y. Kobayashi and M. Unno, Anion recognition by D-ribose-based receptors, *Tetrahedron Lett.*, 2010, **51**, 2512–2514.
38 K. Kano, N. Tanaka and S. Negi, Hydrogen-bonded complexes of carboxylate anions and dextrins in an aprotic polar solvent, *Eur. J. Org. Chem.*, 2001, 3689–3694.
39 J. Seelig and A. Seelig, Lipid conformation in model membranes and biological membranes, *Q. Rev. Biophys.*, 1980, **13**, 19–61.
40 C. Huang, D. Quinn, Y. Sadovsky, S. Suresh and K. Jimmy Hsiaa, Formation and size distribution of self-assembled vesicles, *Proc. Natl. Acad. Sci. U. S. A.*, 2017, **114**, 2910–2915.
41 M. K. Rasmussen, J. N. Pedersen and R. Marie, Size and surface charge characterization of nanoparticles with a salt gradient, *Nat. Commun.*, 2020, **11**, 2337.
42 J. A. Tamada and C. J. King, Extraction of carboxylic acids with amine extractants. 2. Chemical interactions and interpretation of data, *Ind. Eng. Chem. Res.*, 1990, **29**, 1327–1333.
43 S. Jin, J. Zhang, D. Wang, L. Tao, M. Zhou, Y. Shen, Q. Chen, Z. Lin and X. Gao, Structure of six organic acid–base adducts from 6-bromobenzo[*d*]thiazol-2-amine and acidic compounds, *J. Mol. Struct.*, 2014, **1065–1066**, 223–234.
44 M. Widelicka, K. Pogorzelec-Glaser, A. Pietraszko, P. Ławniczak, R. Pankiewiczc and A. Łapiński, Order-disorder phase transition in an anhydrous pyrazole-based proton conductor: the enhancement of electrical transport properties, *Phys. Chem. Chem. Phys.*, 2017, **19**, 25653–25661.
45 K. Wang, M. E. Villanueva, F. Caporaletti, R. P. White, J. E. G. Lipson, S. Napolitano and P. Losada-Pérez, Glassy dynamics as a predictive framework for lipid exchange across membranes, *Small*, 2026, **22**, e12844.